Structure of lateral inhibition in an olfactory bulb model

Andrew Davison, Jianfeng Feng, and David Brown

Laboratory of Computational Neuroscience, The Babraham Institute,
Babraham, Cambridge, CB2 4AT, UK**

Abstract. It has been shown that mutual lateral inhibition of the projection neurones in the olfactory bulb, mediated by interneurones, serves to tune the representation of odours in the bulb and reduce the overlap between similar odorants. In this paper we demonstrate that the parameters of the lateral interaction, specifically the relation of synaptic strength to cell separation and the effective overall gain of the network, have a significant effect on the strength and range of lateral inhibition in a simple model of the olfactory bulb.
Preprint of Davison A.P., Feng J. and Brown D. (1999) Lecture Notes in Computer Science 1606: 189-196

1 Introduction

The dendrodendritic synaptic interaction between mitral/tufted cells and granule cells is a key element in the information processing role of the olfactory bulb [4]. Mitral/tufted cells form reciprocal synapses with granule cells. At these synapses there is a graded, voltage-dependent release of glutamate from mitral cells, and a graded release of GABA from granule cells – mitral cells excite and are inhibited by granule cells. It is hypothesized that this arrangement leads to both reciprocal synaptic inhibition (the mitral cell inhibits itself via the granule cells) and lateral inhibition (the mitral cell inhibits neighbouring mitral cells via the granule cells).

The function of lateral inhibition at this level in the olfactory bulb may be to refine the odour representation by making it more sparse and reducing the overlap with the representations of similar odours [2] [5]. However, little or nothing is known about how the strength of synaptic connections varies with distance along the secondary dendrites. This may have important consequences for the strength and distribution of lateral inhibition, which in turn has implications for the coding of odour by position in the olfactory bulb.

In this paper we have analyzed how the effective network gain and the variation of synaptic strength with range affect the strength and range of the lateral inhibition, using a simple rate model. Our conclusion is that these parameters have a significant effect on the range at which maximum inhibition occurs, on the strength of the inhibition and on 'rebound' disinhibition, and therefore on the odour coding strategies used by the olfactory system.

2 Description of the model

The model closely follows that of Linster and Gervais (1996) [2] and Linster and Hasselmo (1997) [3], but without modulation by centrifugal inputs. It consists of a linear array of n mitral cells and a linear array of n granule cells. The arrays are cyclic,

** Please address correspondence to andrew.davison@yale.edu

i.e. the first cell is adjacent to the last cell. Each cell is modelled as a "point", i.e. details of dendrites, soma and axon are not included. The mitral cells receive sensory input from the olfactory receptor cells, which are not modelled explicitly. Each mitral cell makes excitatory synaptic connections with all granule cells within a certain range of cells either side and receives inhibitory synaptic input from the same granule cells. Each mitral cell also has an excitatory connection to itself.

The "output activity", $V_i^{\mathrm{m}}(t)$ of each mitral cell i varies with time as follows:

$$\tau_{\mathrm{m}} \frac{dV_i^{\mathrm{m}}(t)}{dt} + V_i^{\mathrm{m}}(t) = f_{\mathrm{m}}\left(I_i^{\mathrm{m}}(t)\right) \tag{1}$$

where τ_{m} is the membrane time constant, $I_i^{\mathrm{m}}(t)$ is the total excitatory and inhibitory input to cell i and the gain function $f_{\mathrm{m}}(\cdot)$ is a sigmoid:

$$f_{\mathrm{m}}(x) = \frac{\gamma_{\mathrm{m}}}{1 + \exp\left(-\beta_{\mathrm{m}}\left(x - x_{0\mathrm{m}}\right)\right)} \tag{2}$$

The same equations apply to granule cells, replacing the sub/superscript m with g.

The total inputs are given by:

$$I_i^{\mathrm{m}}(t) = \xi_i(t) + w_s V_i^{\mathrm{m}}(t) - \sum_j w_{ij}^{\mathrm{gm}} V_j^{\mathrm{g}}(t - d_{ij}^{\mathrm{gm}}) \tag{3}$$

$$I_i^{\mathrm{g}}(t) = \sum_j w_{ij}^{\mathrm{mg}} V_j^{\mathrm{m}}(t - d_{ij}^{\mathrm{mg}}) \tag{4}$$

where ξ_i is the sensory input to cell i, w_{ij}^{gm} (w_{ij}^{mg}) and d_{ij}^{gm} (d_{ij}^{mg}) are the weight and time-delay of the synapse *to* mitral (granule) cell i *from* granule (mitral) cell j and w_s is the weight of the mitral cell self-excitation. All weights are positive.

Simulations (not shown here) show that $\boldsymbol{V}_{\mathrm{m}}$ converges either to a fixed point or to a limit cycle. Although there is increasing evidence of the importance of temporal aspects in olfactory processing (see Laurent 1996 for a review [1]) we follow Linster and co-workers and consider only the fixed point equilibrium of the system. At the fixed point equilibrium, $dV_i^{\mathrm{m}}/dt = dV_i^{\mathrm{g}}/dt = 0$, $V_i^{\mathrm{m}}(t - d_{ij}^{\mathrm{mg}}) = V_i^{\mathrm{m}}(t)$ and $V_i^{\mathrm{g}}(t - d_{ij}^{\mathrm{gm}}) = V_i^{\mathrm{g}}(t)$ for all cells i, j. Equations (1), (3) and (4) then become (in vector notation)

$$\boldsymbol{V}_{\mathrm{m}} = f_{\mathrm{m}}\left(\boldsymbol{\xi} + \mathbf{W_s}\boldsymbol{V}_{\mathrm{m}} - \mathbf{W_{gm}}\boldsymbol{V}_{\mathrm{g}}\right) \tag{5}$$

$$\boldsymbol{V}_{\mathrm{g}} = f_{\mathrm{g}}\left(\mathbf{W_{mg}}\boldsymbol{V}_{\mathrm{m}}\right) \tag{6}$$

3 Analysis

We make the assumption that the model operates within the approximately linear part of the sigmoid function and replace this function with:

$$f_{\mathrm{m}}^{linear}(x) = \frac{\beta_{\mathrm{m}}\gamma_{\mathrm{m}}}{4}(x - x_{0\mathrm{m}}) + \frac{\gamma_{\mathrm{m}}}{2} \tag{7}$$

for mitral cells (and similarly for granule cells), which has the same gradient as the non-linear version at $x = x_0$. Therefore, equations (5) and (6) for the equilibrium output of the model become:

$$\boldsymbol{V}_{\mathrm{m}} = \frac{\beta_{\mathrm{m}}\gamma_{\mathrm{m}}}{4}\left(\boldsymbol{\xi} + \mathbf{W_s}\boldsymbol{V}_{\mathrm{m}} - \mathbf{W_{gm}}\boldsymbol{V}_{\mathrm{g}} - x_{0\mathrm{m}}\mathbf{1}\right) + \frac{\gamma_{\mathrm{m}}}{2}\mathbf{1} \tag{8}$$

$$\boldsymbol{V}_{\mathrm{g}} = \frac{\beta_{\mathrm{g}}\gamma_{\mathrm{g}}}{4}\left(\mathbf{W_{mg}}\boldsymbol{V}_{\mathrm{m}} - x_{0g}\mathbf{1}\right) + \frac{\gamma_{\mathrm{g}}}{2}\mathbf{1} \tag{9}$$

where $\mathbf{1}$ is a vector with all elements equal to 1.

The solution for $\boldsymbol{V}_{\mathrm{m}}$ is:

$$\begin{aligned}\boldsymbol{V}_{\mathrm{m}} = &\left[\frac{4}{\beta_{\mathrm{m}}\gamma_{\mathrm{m}}}\mathbf{I} - \mathbf{W_s} + \frac{\beta_{\mathrm{g}}\gamma_{\mathrm{g}}}{4}\mathbf{W_{gm}}\mathbf{W_{mg}}\right]^{-1} \\ &\times\left(\boldsymbol{\xi} + \gamma_{\mathrm{g}}\left(\frac{\beta_{\mathrm{g}}x_{0g}}{4} - \frac{1}{2}\right)\mathbf{W_{gm}}\mathbf{1} + \left(\frac{2}{\beta_{\mathrm{m}}} - x_{0\mathrm{m}}\right)\mathbf{1}\right)\end{aligned} \tag{10}$$

where $\mathbf{I}$ is the identity matrix. This solution is of the form

$$\boldsymbol{V}_{\mathrm{m}} = \mathbf{A}^{-1}\boldsymbol{\xi} + k_1\mathbf{1} \tag{11}$$

where k_1 is a scalar constant. The solution for $\boldsymbol{V}_{\mathrm{g}}$ is:

$$\boldsymbol{V}_{\mathrm{g}} = \frac{\beta_{\mathrm{g}}\gamma_{\mathrm{g}}}{4}\mathbf{W_{mg}}\mathbf{A}^{-1}\boldsymbol{\xi} + k_2\mathbf{1} \tag{12}$$

where k_2 is another scalar constant.

Clearly, the shape of the output vector depends on both the shape of the inverse matrix $\mathbf{A}^{-1}$ and on the shape of the input. We examine the inverse matrix first.

3.1 Shape of the inverse matrix

What is the shape of $\mathbf{A}^{-1}$? We re-write $\mathbf{A}$ in the form:

$$\mathbf{A} = k_3\left(\mathbf{I} + \alpha\widehat{\mathbf{W}}\right) \tag{13}$$

where $\widehat{\mathbf{W}}$ is normalised such that the column sums are all equal to 1, k_3 is a scalar constant and α is defined by:

$$\alpha = \frac{\beta_{\mathrm{g}}\gamma_{\mathrm{g}}\sigma}{4\left(\frac{4}{\beta_{\mathrm{m}}\gamma_{\mathrm{m}}} - w_s\right)} \tag{14}$$

where σ is a scale factor such that $\mathbf{W} = \mathbf{W_{gm}}\mathbf{W_{mg}} = \sigma\widehat{\mathbf{W}}$. The parameter α can be interpreted as the effective gain of the system, since it is increased by increasing the parameters of the sigmoid gain functions $f_{\mathrm{m}}()$ and $f_{\mathrm{g}}()$, by increasing the amplitude of the synaptic weights and by increasing the self-excitation of the mitral cells (provided α remains positive).

Clearly, the shape of $\mathbf{A}^{-1}$ depends on the shape of $\widehat{\mathbf{W}}$. We make the assumptions that synaptic interactions are local and that the synaptic weight between two cells at positions i and j in the array depends only on $|i-j|$. Given these two assumptions, the weight matrices are symmetric and have elements which are constant along diagonals (they are Toeplitz matrices). If the array is cyclic then all rows (and columns) of the matrices have the same shape, centred on the diagonal. We have examined a number of possibilities for the shape of $\mathbf{W}$:

$\mathbf{W_{bell}}$ This is the form used by Linster and Gervais [2]. The elements w_{ij}^{mg} of $\mathbf{W_{mg}}$ decrease linearly with $|i-j|$ out to zero at $|i-j| = r$, where r is the range of synaptic connections, and the elements w_{ij}^{gm} of $\mathbf{W_{gm}}$ constant out to range r. This gives $\mathbf{W_{gm}}\mathbf{W_{mg}}$ a bell-like shape.

$\mathbf{W_{lin}}$ $w_{ij}^{lin} = w_{ij}^{\mathrm{mg}}$
$\mathbf{W_{const}}$ $w_{ij}^{\mathrm{const}} = 1$ for $|i-j| \leq r/2$, $w_{ij}^{\mathrm{const}} = 0$ for $|i-j| > r/2$
$\mathbf{W_{exp}}$ $w_{ij}^{\mathrm{exp}} = \exp\left(-(|i-j|/r)\ln 2\right)$.
$\mathbf{W_{parab}}$ $w_{ij}^{\mathrm{parab}} = 1 - |i-j|^2/2r^2$ for $|i-j| \leq r\sqrt{2}$, $w_{ij}^{\mathrm{parab}} = 0$ for $|i-j| > r\sqrt{2}$

The full-width-at-half-maximum of the row vectors of all the above matrices equals r.

The 'shape' of the inverse matrix depends on (i) α, (ii) the range of synaptic connections relative to the size of the cell array and (iii) the 'shape' of the weight matrix $\mathbf{W}$. The most significant of these parameters is α .

Small α Consider the following algebraic identity:

$$(\mathbf{I}-\mathbf{C})\left(\mathbf{I}+\mathbf{C}+\mathbf{C}^2+\cdots+\mathbf{C}^{m-1}\right) = \mathbf{I}-\mathbf{C}^{\mathrm{m}} \tag{15}$$

It can be shown that if the column sums in $\mathbf{C}$ are all strictly less than 1, then $\mathbf{I}-\mathbf{C}^{\mathrm{m}} \rightarrow \mathbf{I}$ as $m \rightarrow \infty$. In that case, $(\mathbf{I}-\mathbf{C})$ is invertible and, using Eq.(15),

$$(\mathbf{I}-\mathbf{C})^{-1} = \mathbf{I}+\mathbf{C}+\mathbf{C}^2+\cdots \tag{16}$$

Hence, since the column sums of $\widehat{\mathbf{W}}$ are normalised to 1,

$$\left(\mathbf{I}+\alpha\widehat{\mathbf{W}}\right)^{-1} = \mathbf{I}-\alpha\widehat{\mathbf{W}}+\alpha^2\widehat{\mathbf{W}}^2-\cdots \tag{17}$$

provided $\alpha < 1$.

Larger α For $\alpha > 1$, the inverse $\left(\mathbf{I}+\alpha\widehat{\mathbf{W}}\right)^{-1}$ must be found numerically. In general, as α is increased, the number of times the column vector function crosses zero increases, although there are exceptions to this. A typical pattern of behaviour is shown in figure 1: at low α the central 'spike' sits in a large trough. As α increases, the central 'spike' moves upward, creating two new troughs to either side. The height of the spike remains approximately constant, but the amplitudes of the peaks and troughs increase to infinity. At a critical value of α (approximately 29.48 in this case) the curve inverts and the spike is now at the bottom of a trough. The amplitudes of the peaks and troughs now diminish again and the process repeats, the curve inverting at $\alpha \simeq 600-650$ and $\alpha \simeq 900-1000$. Figure 2 plots the value of the central (spike) element of the vector as a function of α. It clearly shows the divergence of the curve maximum at $\alpha \simeq 30, 600-650$ and $900-1000$.

Similar behaviour is found for $\mathbf{W_{gauss}}$, $\mathbf{W_{parab}}$ and $\mathbf{W_{const}}$ for the same range, although the values of α at which the maximum $\rightarrow \infty$ are different.

For smaller ranges a different behaviour is seen at low α: again the number of zero crossings increases, but the central spike is always sitting in a trough, the depth of which increases and the width decreases as α increases (figure 3). This behaviour may persist as $\alpha \rightarrow \infty$ if the range is small enough, otherwise the previously described behaviour begins at higher α.

$\mathbf{W_{lin}}$ and $\mathbf{W}_{\mathrm{exp}}$ exhibit this second behaviour for large values of the range r as well as for small values.

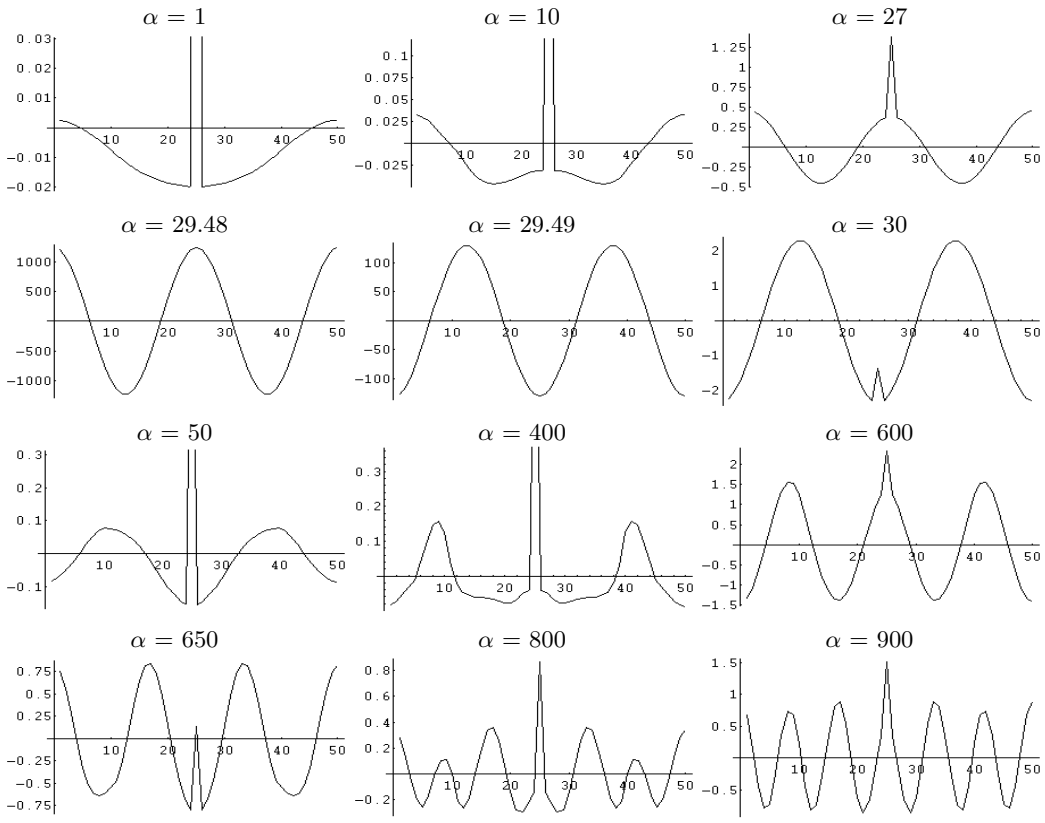

Fig. 1. A row vector of $(\mathbf{I}+\alpha\widehat{\mathbf{W}})^{-1}$ for $\mathbf{W} = \mathbf{W_{bell}}$, $r = 30$, $n = 50$

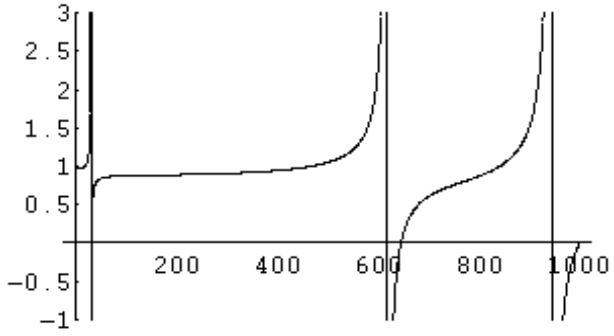

Fig. 2. Variation of $\max[(\mathbf{I}+\alpha\widehat{\mathbf{W}})^{-1}]$ with α for $\mathbf{W} = \mathbf{W_{bell}}$, $r = 30$, $n = 50$

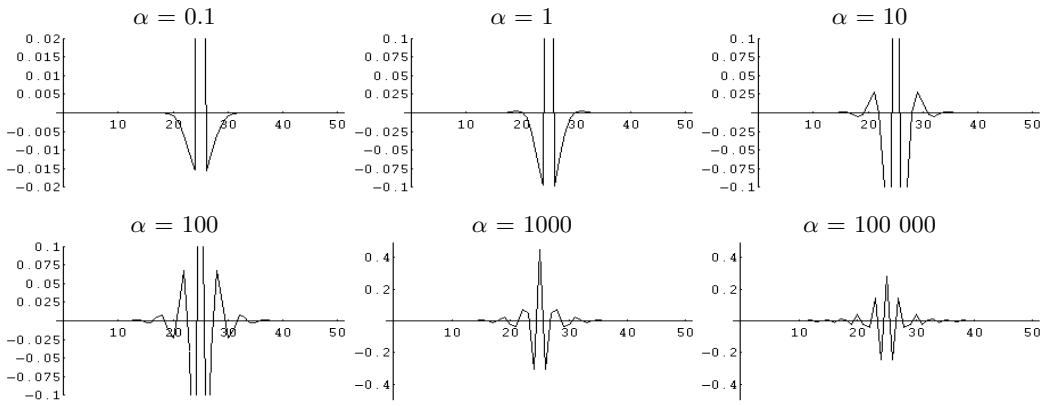

Fig. 3. A row vector of $(\mathbf{I}+\alpha\widehat{\mathbf{W}})^{-1}$ for $\mathbf{W} = \mathbf{W_{gauss}}$, $r = 5$, $n = 50$

3.2 Input-Output relations

The previous section has shown that $\mathbf{A}^{-1}$ can have very varied shapes, particularly for large values of α , but what is the effect of the shape of $\mathbf{A}^{-1}$ on the output vector, for a given input vector? We considered two possibilities for the input vector: $\boldsymbol{\xi}_{\mathbf{square}}(i,r)$ and $\boldsymbol{\xi}_{\mathbf{gauss}}(i,r)$. $\boldsymbol{\xi}_{\mathbf{square}}(i,r)$ ("square input") has r consecutive elements equal to 1, centred on cell i, all other input elements are zero. $\boldsymbol{\xi}_{\mathbf{gauss}}(i,r)$ ("gaussian input") has a gaussian shape, maximum equal to 1, centred on cell i. Except where indicated, all results in this section were obtained for $\mathbf{W} = \mathbf{W_{bell}}$.

With the square input, the general form of the output vector is a modified box shape with a central depression, peripheral peaks and surrounding depressions (Figure 4(a) and 4(b)). With smaller values of the range parameter, sub-peaks appear within the central depression. The main effect of increasing α is to deepen the depressions (compare figure 4(a) and (b) with 4(c) and (d)). With the gaussian input, the general form of the output vector is a "Mexican hat" shape (Figure 4, fourth column). The width of the output peak is always less than that of the input peak. Increasing α decreases the width of the output peak. Increasing the range r increases both the absolute value of the central peak and the ratio of the peak height to the depth of the surrounding depressions. Increasing r also increases the width of the depressions, i.e. increases the range within which cells are suppressed.

Using $\mathbf{W_{exp}}$ rather than $\mathbf{W_{bell}}$ has little effect on the output, particularly for small α , despite the rather large difference in $\mathbf{A}^{-1}$ (for example see figure 4(e) and (f) for 'gaussian' input). The small difference is less pronounced inhibition but with a larger range.

4 Discussion

When the gain parameter α is small a 'classical' form of lateral inhibition is found, in which a mitral cell's nearest neighbours are most inhibited, and this inhibition falls off with distance. However, when α is larger the nearest neighbours may be potentiated and only more distant cells be inhibited, depending on how synaptic strength varies along the secondary dendrites. The parameter values given in Linster and Hasselmo (1997) [3] give α around 0.3, which is a 'small' value in this context. What a realistic value might be for the real biological system is difficult to estimate, as it depends on

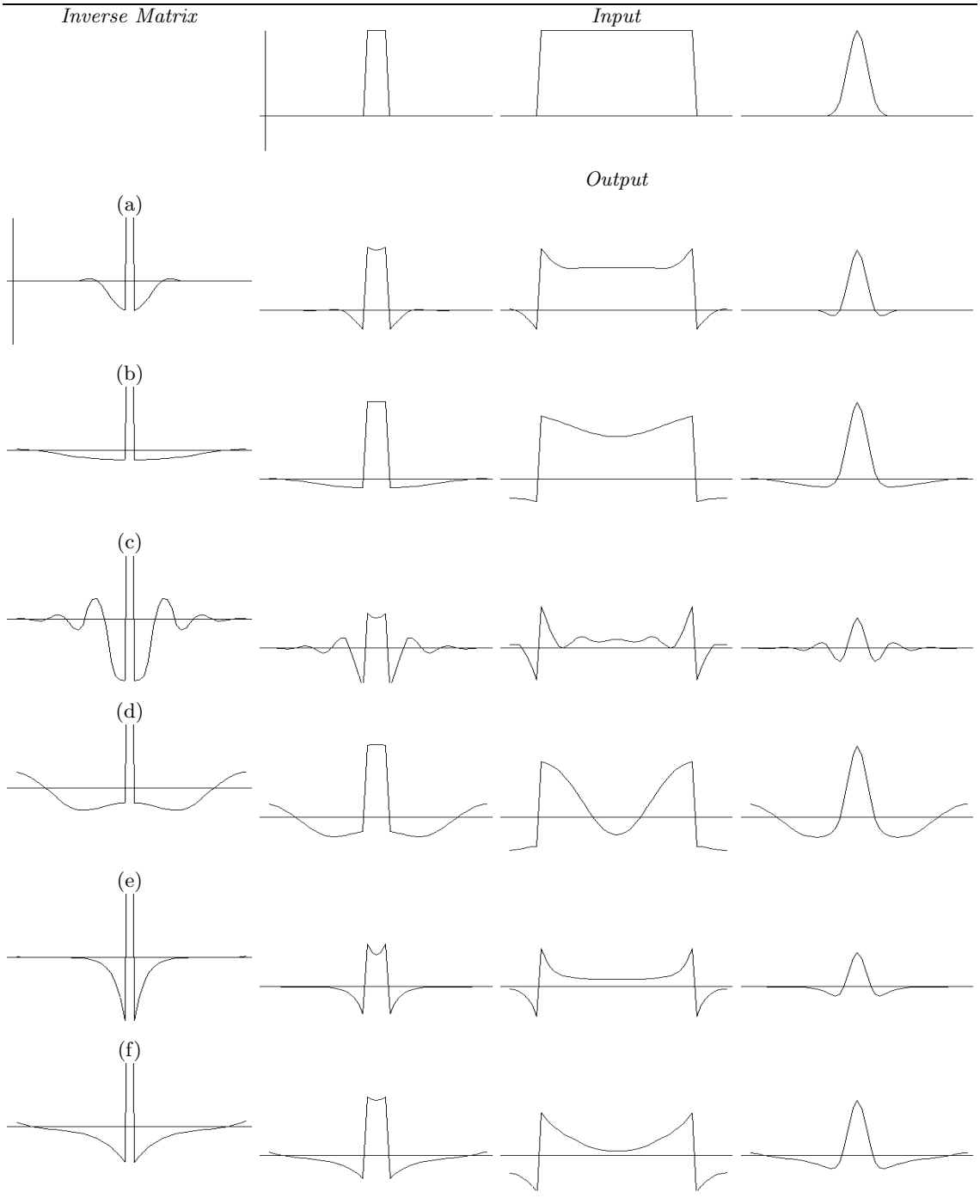

Fig. 4. Input-Output relations for 'square' and 'gaussian' inputs with either bell-shaped or exponential lateral connectivity: (a) $(\mathbf{I} + \mathbf{W_{bell}})^{-1}, r = 10$ (b) $(\mathbf{I} + \mathbf{W_{bell}})^{-1}, r = 30$ (c) $(\mathbf{I} + 10\mathbf{W_{bell}})^{-1}, r = 10$ (d) $(\mathbf{I} + 10\mathbf{W_{bell}})^{-1}, r = 30$ (e) $(\mathbf{I} + 10\mathbf{W_{exp}})^{-1}, r = 10$ (f) $(\mathbf{I} + 10\mathbf{W_{exp}})^{-1}, r = 30$. x-scale (cell number) 1–50, y-scale -0.13–+0.13 (column 1), -0.4–1.0 (columns 2-4)

experimentally unknown details of neurotransmitter release, post-synaptic properties and active membrane properties.

Both α and the variation in effective synaptic strength along the secondary dendrites of mitral cells can have large effects on the properties of lateral inhibition, and hence the information coding/filtering properties of the olfactory bulb. When assessing possible coding strategies, or the effects of learning, in the olfactory system, this needs to be taken into account. In future work we will investigate the interaction of lateral inhibition with olfactory learning, and their influences on the dynamic properties of the model.

References

1. G. Laurent. Dynamical representation of odors by oscillating and evolving neural assemblies. *Trends in Neuroscience*, 19:489–496, 1996.
2. C. Linster and R. Gervais. Investigation of the role of interneurons and their modulation by centrifugal fibres in a neural model of the olfactory bulb. *Journal of Computational Neuroscience*, 3:225–246, 1996.
3. C. Linster and M. Hasselmo. Modulation of inhibition in a model of olfactory bulb reduces overlap in the neural representation of olfactory stimuli. *Behavioural Brain Research*, 84:117–127, 1997.
4. G. M. Shepherd. *The Synaptic Organization of the Brain*. Oxford University Press, Oxford, 3rd edition, 1990.
5. M. Yokoi, K. Mori, and S. Nakanishi. Refinement of odor molecule tuning by dendrodendritic synaptic inhibition in the olfactory bulb. *Proc. Natl. Acad. Sci. USA*, 92:3371–3375, 1995.